NASA TECHNICAL NOTE

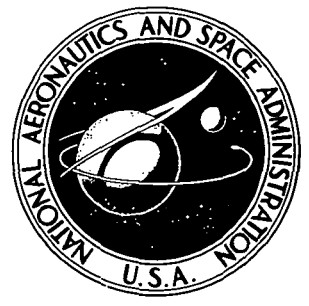

NASA TN D-7185

NASA TN D-7185

THEORETICAL AND EXPERIMENTAL INTERNAL FLOW CHARACTERISTICS OF A 13.97-CENTIMETER-DIAMETER INLET AT STOL TAKEOFF AND APPROACH CONDITIONS

by James A. Albers

Lewis Research Center
Cleveland, Ohio 44135

NATIONAL AERONAUTICS AND SPACE ADMINISTRATION • WASHINGTON, D. C. • MARCH 1973

1. Report No.	2. Government Accession No.	3. Recipient's Catalog No.
NASA TN D-7185		

4. Title and Subtitle	5. Report Date
THEORETICAL AND EXPERIMENTAL INTERNAL FLOW CHARACTERISTICS OF A 13.97-CENTIMETER-DIAMETER INLET AT STOL TAKEOFF AND APPROACH CONDITIONS	March 1973
	6. Performing Organization Code

7. Author(s)	8. Performing Organization Report No.
James A. Albers	E-7237
	10. Work Unit No. 501-24
9. Performing Organization Name and Address Lewis Research Center National Aeronautics and Space Administration Cleveland, Ohio 44135	11. Contract or Grant No.
	13. Type of Report and Period Covered Technical Note
12. Sponsoring Agency Name and Address National Aeronautics and Space Administration Washington, D.C. 20546	14. Sponsoring Agency Code

15. Supplementary Notes

16. Abstract

The theoretical and experimental internal flow characteristics of a 13.97-cm-diam inlet with centerbody retracted and extended are presented at STOL takeoff and approach operating conditions. The theoretical results were obtained from incompressible potential flow corrected for compressibility and boundary layer. Comparisons between theoretical internal surface static-pressure distributions and experimental data are presented for free-stream velocities of 0, 24, 32, and 45 m/sec for a range of inlet incidence angles from 0 to 50°. Surface static-pressure distributions are illustrated at circumferential locations of 0, 60°, 120°, and 180°. Surface Mach number distributions from the stagnation point to the diffuser exit are presented along with turbulent boundary-layer shape factors. In general, good agreement was found between the theoretical and experimental surface static pressure distributions.

17. Key Words (Suggested by Author(s))	18. Distribution Statement
Inlet design; Sonic inlet; Induction system; Pressure distribution; Potential flow; Boundary layer flow; Compressibility correction; STOL aircraft	Unclassified - unlimited

19. Security Classif. (of this report)	20. Security Classif. (of this page)	21. No. of Pages	22. Price*
Unclassified	Unclassified	22	$3.00

* For sale by the National Technical Information Service, Springfield, Virginia 22151

THEORETICAL AND EXPERIMENTAL INTERNAL FLOW CHARACTERISTICS OF A 13.97-CENTIMETER-DIAMETER INLET AT STOL TAKEOFF AND APPROACH CONDITIONS

by James A. Albers

Lewis Research Center

SUMMARY

The theoretical and experimental internal flow characteristics of a 13.97-centimeter-diameter inlet with centerbody retracted and extended are presented at STOL takeoff and approach operating conditions. The theoretical results are obtained from incompressible potential flow corrected for compressibility and boundary layer. Comparisons between theoretical internal surface pressure distributions and experimental data are presented for free-stream velocities of 0, 24, 32, and 45 meters per second for a range of inlet incidence angles from 0 to 50°. Surface static-pressure distributions are illustrated at circumferential locations of 0, 60°, 120°, and 180°. Surface Mach number distributions from stagnation point to diffuser exit are presented along with turbulent boundary layer shape factors.

The results indicate a large circumferential variation in surface static pressures at the inlet highlight and throat at large incidence angles. Only small circumferential variations in surface static pressure occurred in the last 50 percent of the diffuser. The largest diffuser adverse pressure gradients occurred on the windward side of the inlet and at the highest incidence angle. A 45-percent increase in local surface Mach number (52-percent decrease in surface static pressure) was obtained as incidence angle was increased from 0 to 40°. Local theoretical surface Mach numbers as high as 1.45 were found on the windward side of the inlet. Extending the centerbody of the inlet forward resulted in large regions of local sonic velocities in the throat of the inlet. In general, the theoretical and experimental surface static pressure distributions agreed. However, at the inlet highlight the theoretical static pressures were generally lower than the experimental data.

INTRODUCTION

Currently, there is much interest in the design and understanding of inlets for subsonic aircraft. The inlet must be designed to supply high pressure recovery and uniform flow to the engine compressor during low-speed and cruise operation. Engine operation can be adversely affected by circumferential distortions, occurring mainly when the airplane is operating at high angles of attack or yaw (ref. 1). Because of the high lift coefficients and low speed necessary for takeoff and landing operation of STOL aircraft, the engine inlet will be exposed to larger upwash angles than conventional aircraft (ref. 2). In addition, the engine inlet may be exposed to crosswinds as large as 13 to 18 meters per second (ref. 3). These large incidence angles result in large adverse pressure gradients over a large portion of the internal diffuser surface. These large adverse pressure gradients may cause either laminar or turbulent separation. In general, the designer tries to avoid flow separation on the inlet surface in order to achieve high pressure recovery and uniform flow at the compressor face. Little experimental information on nacelle inlets at incidence angles other than zero is currently available. Also, accurate methods for estimating surface pressure distributions and boundary layer characteristics are needed to do detailed design studies of inlets for STOL aircraft.

This report presents theoretical and experimental internal flow characteristics of a 13.97-centimeter-diameter inlet at STOL takeoff and approach conditions. The theoretical methods used in this investigation include both potential flow and boundary-layer flow for axisymmetric inlets. The experimental data were obtained from wind tunnel tests of the translating centerbody inlet reported in reference 4. The inlet configuration (fig. 1) is a representative geometry for STOL applications. Details of the inlet geometry are given in reference 4. Comparisons between internal surface pressure distributions and experimental data are presented for free stream velocities of 0, 24, 32, and 45 meters per second for a range of incidence angles from 0 to 50°. Mass flow rates through the inlet ranged from 90 to 103 percent of design. The design corrected flow rate was 2.49 kilograms per second. Location of stagnation points on the inlet lip and surface Mach number distributions are presented along with turbulent boundary-layer shape factors. The effect of centerbody location on surface static pressures is also illustrated.

METHOD OF ANALYSIS

The incompressible potential flow solution for axisymmetric inlets is the basis of an analytical tool to design inlets for STOL applications. The incompressible potential

flow solution was obtained by the method of reference 5. This solution yields velocity and static pressures on the surface of the inlet for any combination of free-stream velocity, inlet incidence angle, and mass flow rate through the inlet. The method of reference 5 is based on the Douglas potential flow method (ref. 6). The incompressible potential flow solution can be refined by including the effects of compressibility and boundary layer.

Compressibility Correction

High subsonic or supersonic flows exist on STOL engine inlets at takeoff and approach operating conditions. Thus, a compressibility correction should be made to the incompressible velocity. A compressibility correction applicable to nacelle inlets is discussed in reference 7, which proposed an empirical relation between the local incompressible velocity V_i and the local compressible velocity V_c. It is expressed as

$$V_c = V_i \left(\frac{\rho_i}{\overline{\rho}_c} \right)^{(V_i/\overline{V}_i)} \tag{1}$$

where

ρ_i incompressible density, which is equal to stagnation density

$\overline{\rho}_c$ average compressible density across flow passage

$\overline{V}_i$ average incompressible velocity across flow passage at given station

This relation was used in this investigation.

Boundary-Layer Flow

The surface Mach number distributions obtained from the potential flow solution were used as an input to the boundary-layer analysis to determine its growth and separation (if any) on the inlet surface. The method of Herring and Mellor (ref. 8) was chosen to calculate both laminar and turbulent boundary-layer growth because of its accuracy, physical soundness, and adaptability to the present problem. The effective-viscosity hypothesis of Mellor and Herring should be applicable for high adverse gradient flows encountered for inlets during low-speed operation. A more detailed discussion of this hypothesis is given in reference 9.

In order to compute a boundary-layer solution, it was necessary to prescribe the velocity profile at the start of the calculation, namely, the stagnation point on the inlet. Because the flow in the immediate neighborhood of the forward stagnation point is both laminar and incompressible, laminar similarity solutions were applicable. The Falkner-Skan laminar wedge flow solution (ref. 10) for stagnation point flow was used for a starting profile. This initial profile was calculated in the computer program of reference 8.

In addition, the transition point from laminar to turbulent flow must be located. The location of the transition point was based on theoretical considerations because of the lack of empirical methods that were applicable to the present problem. According to Schlichting (ref. 10) the point of transition in the range of Reynolds numbers from 10^6 to 10^7 almost coincides with the point of minimum pressure of the potential flow. In this report the transition was assumed to take place at the point of minimum pressure.

Once the laminar and turbulent boundary-layer characteristics on the inlet lip and diffuser are calculated, the location of the turbulent separation point (if any) can be determined. The criteria used for turbulent separation are as follows: (1) adverse pressure gradient; (2) skin friction coefficient of approximately zero; (3) increase in shape factor H as the separation point is approached; (4) a value of H of 2.6 or greater immediately ahead of the separation point.

RESULTS AND DISCUSSION

Surface Static-Pressure Distributions

Theoretical surface static-pressure distributions are first compared with experimental data for conditions where the flow is generally well behaved (i.e., attached along the inlet surface). The two inlet geometries considered are shown in figure 1. All data comparisons are made for the inlet with centerbody retracted (fig. 1(a)) unless stated otherwise. The effects of compressibility and boundary-layer displacement thickness correction on the incompressible potential flow solution are first discussed.

Effect of compressibility correction. - A comparison of the theoretical internal surface static-pressure distributions with experimental data is shown in figure 2 for static conditions ($V_\infty = 0$). (Symbols are defined in the appendix.) The pressure distributions are presented from the inlet highlight ($X/L = 0$) to the diffuser exit ($X/L = 1.0$). The incompressible potential flow solution (the dashed line) yields static pressures approximately 12 percent higher than experimental data near the inlet highlight and approximately 5 percent higher in the aft portion of the diffuser. The incompressible potential flow solution overestimates the static pressure because of the high surface Mach numbers (up to 0.9). The incompressible potential flow solution with the compressibility

correction is shown in figure 2 (solid line). The theory with the compressibility correction generally compares well with the experimental data in the first half of the inlet. However, in the aft portion of the diffuser the theoretical static pressures are up to 3 percent higher than experimental data.

Effect of boundary-layer displacement thickness correction. - A combined potential flow and boundary-layer analysis improves the agreement between the experimental and theoretical surface static-pressure distributions in the aft portion of the diffuser. This is illustrated for a static condition ($V_\infty = 0$) in figure 3(a) and for a free-stream velocity of 24 meters per second at an incidence angle of 40° in figure 3(b). Adding the theoretical boundary-layer displacement thickness to the inlet surface results in a decreased flow passage cross-sectional area and hence an increase in the local surface Mach number. The boundary layer is thickest near the diffuser exit and hence affects the static pressure most in this region. The increase in local surface Mach number yields a reduced theoretical surface static pressure for the potential flow solution with a boundary-layer correction.

With both the compressibility correction and boundary-layer correction, the theoretical and experimental static pressures are in good agreement over the entire length of the diffuser. The boundary-layer correction is also effective in improving the solution at incidence angle (fig. 3(b)) in spite of the fact the boundary layer is not uniformly distributed circumferentially in the aft portion of the diffuser.

The boundary-layer correction is not included in the remaining theoretical static pressures because of the large computation time required to make this correction. Hence, there are small discrepancies between the theory and experiment in the aft portion of the diffuser in the subsequent figures.

Circumferential variation. - The variation of the theoretical internal surface static pressure along the diffuser surface for several circumferential angles ψ and for incidence angles of 20° and 40° is presented in figure 4. The circumferential variation in static pressure is greatest at the inlet highlight ($X/L = 0$) and decreases with increasing X/L. The circumferential variation in p/P_∞ is small for X/L locations greater than 0.5. The degree of the circumferential variation in static pressure increases as incidence angle is increased. At the inlet throat a 9 percent circumferential variation in p/P_∞ occurs at an incidence angle of 20° (fig. 4(a)), and a 16-percent variation occurs at an incidence angle of 40° (fig. 4(b)).

Both the theoretical and the experimental circumferential variation of static pressure at several stations is shown in figure 5. The experimental static pressures generally compare well with the theoretical pressures for all circumferential angles. The lowest inlet lip static pressures and largest diffuser adverse pressure gradients occur on the windward side of the inlet ($\psi = 0$). Thus, all remaining comparisons will be made at circumferential angle of $\psi = 0$.

Effect of flow variables. - To illustrate the applicability of the prediction method over a wide range of conditions, a comparison with experimental data is made for various incidence angles, free-stream velocities, and mass flow rates. The effect of the three flow variables on the theoretical static pressures is first discussed. This is followed by a discussion of the comparison between theory and experiment.

The effect of incidence angle is illustrated in figure 6 by the theoretical static-pressure distributions (with experimental data) at a free-stream velocity of 32 meters per second and for incidence angles of 0, 20°, and 40°. The value of the static-pressure ratio on the inlet lip decreases considerably as the incidence angle increases from 0 to 40°. For example, the theoretical static-pressure ratio at the inlet highlight decreases from 0.57 at an incidence angle of 0 to 0.30 at an incidence agle of 40°. There is little change in the static-pressure prediction in the aft portion of the diffuser ($X/L > 0.4$) as incidence angle is increased from 0 to 40°. The large decrease in static-pressure ratio as incidence angle increases is related to the shift in the stagnation point on the outer cowl surface on the windward side of the inlet. As the incidence angle increases from 0 (fig. 7(a)) to 40° (fig. 7(c)), the stagnation point moves further under the lower cowl external surface. This results in higher velocities and corresponding lower pressures on the internal surfaces of the inlet. The minimum pressure point on the windward lip moves near the inlet highlight. Figure 7 also illustrates the stagnation points on the leeward side of the inlet.

The effect of free-stream velocity on the static-pressure distribution is illustrated in figure 8 for free-stream velocities of 24, 32, and 45 meters per second at a incidence angle of 0. Small increases in static pressures occur on the inlet lip ($0 < X/L < 0.17$) as the free-stream velocity increased. This result is related to the shift in the stagnation point toward the highlight as the free-stream velocity increases as shown in figure 7.

Shown in figure 9 is a comparison of theoretical static-pressure distributions with experimental data for mass flow rates of 90 and 100 percent of design for angles of incidence of 0, 20°, and 40°. The theoretical static pressure ratio p/P_{∞} at the inlet highlight at static conditions decreases from 0.57 to 0.44 at zero incidence (fig. 9(a)) as the mass flow rate increases from 90 to 100 percent of design. There is approximately a 27-percent increase in the theoretical pressure difference from inlet highlight to diffuser exit for a 10-percent increase in mass flow rate. Similar results exist for 20° and 40° incidence angles (figs. 9(b) and (c)). This indicates the large sensitivity of static-pressure distribution to mass flow rate.

The theoretical surface static pressures generally compare well with experimental data for all free-stream velocities, incidence angles, and mass flow rates (figs. 6, 8, and 9). However, some discrepancy between predicted static pressures and experimental data occur near the inlet highlight. The larger differences occur at the higher inci-

dence angles (figs. 6 and 9(c)). At incidence angles of 20° or greater, the value of the static-pressure ratio indicates local Mach numbers greater than one near the inlet highlight. The possibility of local shocks and/or short separation bubbles and reattachment (often encountered on airfoils at angle of attack) near the inlet highlight could account for the experimental static pressures being higher than the theory.

Effect of centerbody location. - Extending the centerbody forward (fig. 1(b)) results in a larger extent and lower value of static pressure on the inlet lip (fig. 10). This resulted in a larger region of supersonic flow and a 17 percent increase in the static pressure rise for the inlet with the centerbody extended. A discrepancy between data and theory for the centerbody extended was found in the region of the inlet throat ($0 < X/L < 0.2$) for static conditions (fig. 10(a)) and at an incidence angle of 40° (fig. 10(c)). This difference may be due to the presence of a small separation bubble and later reattachment in the inlet throat as the result of the large longitudinal extent of supersonic flow for these conditions. Good agreement was found between data and theory for an incidence angle of 20° (fig. 10(b)) where the longitudinal extent of supersonic flow was small.

Useful range of compressibility correction. - The good agreement between data and theory over a wide range of conditions investigated (figs. 6 and 8 to 10) indicates the applicability of the compressibility correction for high subsonic and transonic flow. In some cases when the longitudinal extent of supersonic flow was small, good agreement was obtained for local Mach numbers as high as 1.3 ($p/P_{\infty} = 0.36$) (figs. 6 and 9(c)). In others, when the longitudinal extent of supersonic flow was large and the centerbody extended, poorer agreement was found between theory and experiment (figs. 10(a) and (c)). At the inlet highlight ($X/L = 0$), the theoretical static pressures were generally lower than experimental data.

Boundary-Layer Characteristics

The Mach number distributions obtained from the potential flow solution were used to determine the boundary-layer growth. Typical distributions along the inlet surface from the stagnation point to the diffuser exit are presented in figure 11 at incidence angles from 0 to 40°. At zero incidence angle, the Mach number increases from zero at the stagnation point to 1.0 within the first 15 percent of the surface distance to the diffuser exit. A 45-percent increase in the peak local surface Mach number (corresponding to a 52-percent decrease in static pressure), occurred as the incidence angle was increased from 0 to 40°. Local Mach numbers as high as 1.45 were calculated at an incidence angle of 40°. The location of the maximum Mach number on the inlet surface (point of minimum pressure) occurs very near the inlet highlight ($X/L = 0$) as pre-

viously shown in figure 7.

Turbulent boundary-layer shape factors (model scale). - Boundary-layer shape factor along the surface of the inlet is indicative of the local boundary-layer characteristics. Inlets should be designed to avoid flow separation by minimizing gradients in and the magnitude of the shape factor along the surface. Typical shape factors based on predicted Mach number distributions are presented in figure 12.

From the point where the turbulent boundary-layer growth starts (X/L = 0), the shape factor decreases along the surface of the diffuser and begins to increase in the aft portion of the diffuser ($S/SM > 0.6$). The higher the incidence angle, the larger the gradient in the shape factor. Boundary-layer separation was not indicated for incidence angles from 0 to 30°. At an incidence angle of 40° and at X/L = 0.62, the shape factor increases to a value of 2.7, and the value of the skin friction coefficient was 0.0001, which indicates diffuser separation. Diffuser separation was not evident from the measured static-pressure distribution of figure 6.

The surface Mach numbers calculated from the experimental static pressures are presented in figure 13 for an incidence angle of 40° and are compared with the theoretical values. The major difference between the two curves is in the region of maximum Mach number (minimum pressure). The maximum measured Mach number was 12 percent lower than the predicted value. When the experimental values of Mach number were used to calculate the shape factors, no separation was predicted as shown in figure 14. This indicates that the minimum surface pressure ratio p/P_{∞} is very critical in determining diffuser separation.

Comparison of model and full-scale shape factors. - Scale effects on the turbulent boundary-layer growth are an important design consideration. A comparison between model and full-scale theoretical shape factors is illustrated in figure 15. The full-scale inlet was taken as 10 times the size of the model (13.97-cm diam). At an incidence angle of 40° there are large gradients in the shape factor that indicate diffuser separation for the model scale. However, separation was not predicted at full scale. The relatively flat profile in the aft portion of the diffuser is the result of the reduced pressure gradient and increased Reynolds number at full scale. These results demonstrate that if the inlet diffuser was designed totally on small-scale experimental data, it would be conservative.

Separated flows. - The majority of the data that has been previously discussed has been for attached flow. We will now consider an example where the experimental static pressures indicate complete inlet separation. This is illustrated in figure 16 for an incidence angle of 50°. The experimental static pressures are relatively flat from inlet highlight to diffuser exit. The theoretical potential flow static pressures predict a large adverse pressure gradient in the inlet throat. Examination of the experimental and theoretical static pressure distributions indicates separation very near the inlet

highlight. The boundary-layer analysis indicated turbulent separation at $X/L = 0.5$. Since transition to turbulent flow was assumed at the minimum pressure point, laminar separation could not be considered in the analysis. Comparing this theoretical separation location ($X/L = 0.5$) with the experimental separation location ($X/L = 0$) indicates that separation was laminar and that accurate methods of determining transition may be required to predict inlet separation near the inlet highlight.

SUMMARY OF RESULTS

The theoretical and experimental internal flow characteristics of an inlet with the centerbody retracted and extended were compared at free-stream velocities of 0, 24, 32, and 45 meters per second and for a range of inlet incidence angles from 0 to 50°. The principal results of this study are as follows:

1. Good agreement between the theoretical surface pressure distribution and experimental data was obtained when compressibility and boundary-layer corrections were included in the theory. In some cases, when the longitudinal extent of supersonic flow was small, good agreement was obtained for local Mach numbers as high as 1.3. In others, when the longitudinal extent of supersonic flow was large and the centerbody extended, poorer agreement was found between theory and experiment. At the inlet highlight ($X/L = 0$) the theoretical static pressures were generally lower than the experimental data.

2. There is a large circumferential variation in surface static pressures at the inlet highlight and throat at large incidence angles. Only small circumferential variation in surface static pressure occurs in the last 50 percent of the diffuser. The largest adverse pressure gradients occurred on the windward side of the inlet and at the highest incidence angle.

3. There was a 45 percent increase in local surface Mach number (52 percent decrease in surface static pressure) near the inlet highlight on the windward side of the inlet as incidence angle was increased from 0 to 40°. Local predicted surface Mach numbers as high as 1.45 were found on the windward side of the inlet surface.

4. The stagnation points occurred on the external cowl surface for all conditions investigated. The higher the free-stream velocity the closer the stagnation point is to the inlet highlight.

5. Extending the centerbody of the inlet forward results in larger regions of supersonic velocities in the throat of the inlet. The theoretical static-pressure rise (from inlet highlight to diffuser exit) for the inlet with the centerbody extended are approximately 17 percent greater than with the inlet retracted.

6. For predicting separation in the diffuser, the minimum pressure ratio p/P_{∞} is

very critical in calculating the inlet boundary-layer growth and separation location.

7. When separated flow near the inlet highlight existed for the experimental data, the boundary-layer analysis (assuming transition at the minimum pressure point) predicted turbulent separation midway between the inlet highlight and diffuser exit. This comparison suggests that accurate methods of determining transition may be required to predict separation near the inlet highlight.

8. Large differences existed between model and full-scale boundary-layer shape factors in the diffuser. If an inlet diffuser is designed totally on small-scale experimental data, it would be conservative.

Lewis Research Center,
National Aeronautics and Space Administration,
Cleveland, Ohio, November 28, 1972,
501-24.

APPENDIX - SYMBOLS

H shape factor, δ^*/θ

L distance from inlet highlight to diffuser exit (fig. 1)

M surface Mach number

P total pressure

p surface static pressure

S local surface distance from stagnation point (fig. 7)

SM total surface distance from stagnation point to diffuser exit (fig. 7)

V velocity

X distance from inlet highlight (fig. 1)

ψ circumferential angle around inlet (fig. 4)

δ^* displacement thickness

θ momentum thickness

ρ density

Subscripts:

c compressible

i incompressible

∞ free stream

Superscript:

$\bar{}$ average value across inlet flow passage

REFERENCES

1. Alford, Joseph S.: Inlet Flow Distortion Index. Presented at the International Days of Aeronautical Sciences, Paris, May 27-29, 1957.

2. Albers, James A.: Predicted Upwash Angles at Engine Inlets for STOL Aircraft. NASA TM X-2593, 1972.

3. Ransone, R. K.: Proposed STOL Definition and Field Length Criteria. J. Aircraft, vol. 8, no. 12, Dec. 1971, pp. 971-976.

4. Miller, Brent A.; and Abbott, John M.: Aerodynamic and Acoustic Performance of Two Choked-Flow Inlets Under Static Conditions. NASA TM X-2629, 1972.

5. Stockman, Norbert O.: Potential Flow Solutions for Inlets of VTOL Lift Fans and Engines. Analytic Methods in Aircraft Aerodynamics. NASA SP-228, 1970, pp. 659-681.

6. Hess, J. L.; and Smith, A. M. O.: Calculation of Potential Flow About Arbitrary Bodies. Progress in Aeronautical Sciences. Vol. 8. D. Küchemann, ed., Pergamon Press, 1967, pp. 1-138.

7. Lieblein, S.; and Stockman, N. O.: Compressibility Correction for Internal Flow Solutions. J. Aircraft, vol. 9, no. 4, Apr. 1972, pp. 312-313.

8. Herring, H. J.; and Mellor, G. L.: Computer Program for Calculating Laminar and Turbulent Boundary Layer Development in Compressible Flow. NASA CR-2068, 1972.

9. Mellor, George L.; and Herring, H. James: Two Methods of Calculating Turbulent Boundary Layer Behavior Based on Numerical Solutions of the Equations of Motion. Methods, Predictions, Evaluation and Flow Structure. Vol. 1 of Computation of Turbulent Boundary Layers. S. J. Kline, M. V. Morkovin, G. Sovran, and D. J. Cockrell, eds., Stanford Univ. Press, 1969, pp. 331-345.

10. Schlichting, Hermann (J. Kestin, trans.): Boundary Layer Theory. Fourth ed., McGraw-Hill Book Co., Inc., 1960, p. 143.

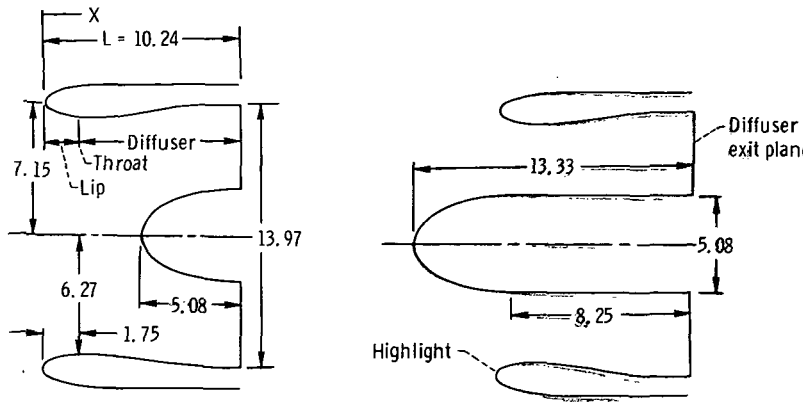

(a) Centerbody retracted. (b) Centerbody extended.

Figure 1. - Translating centerbody inlet. (All dimensions in cm.)

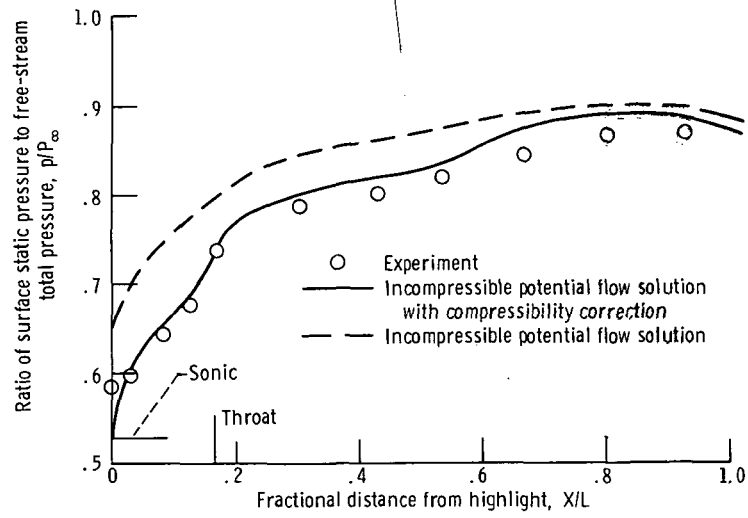

Figure 2. - Effect of compressibility correction on surface static-pressure distribution. Static condition; mass flow rate, 91 percent of design; centerbody retracted.

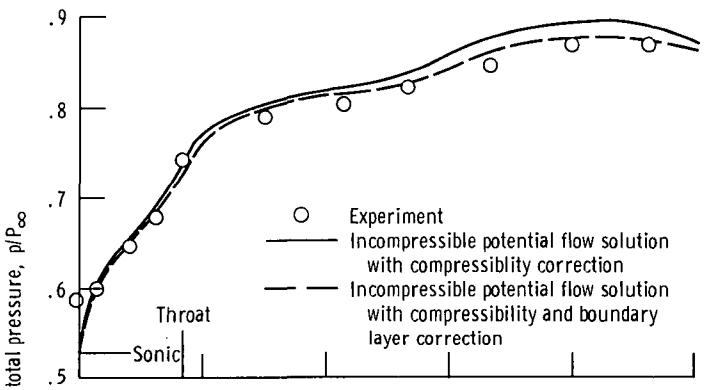

(a) Static condition; mass flow rate, 91 percent of design.

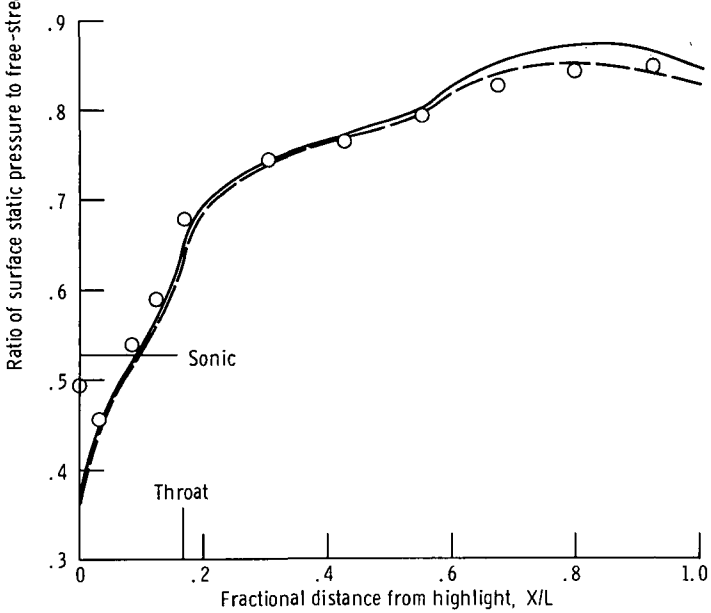

(b) Free-stream velocity, 24 meters per second; incidence angle, 40^0; mass flow rate, 102 percent of design; circumferential angle, 0.

Figure 3. - Effect of boundary-layer displacement thickness correction on surface static-pressure distribution. Centerbody retracted.

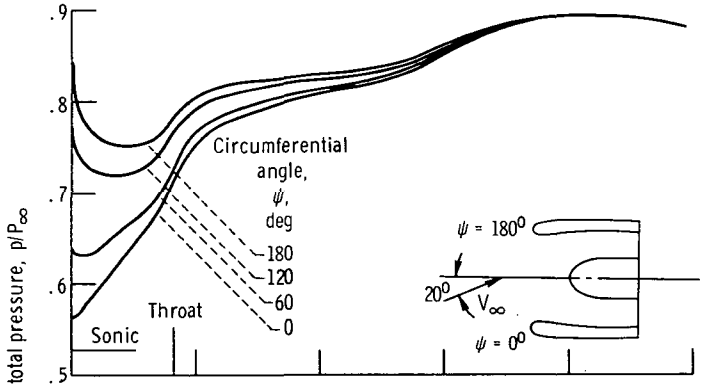

(a) Incidence angle, 20^0.

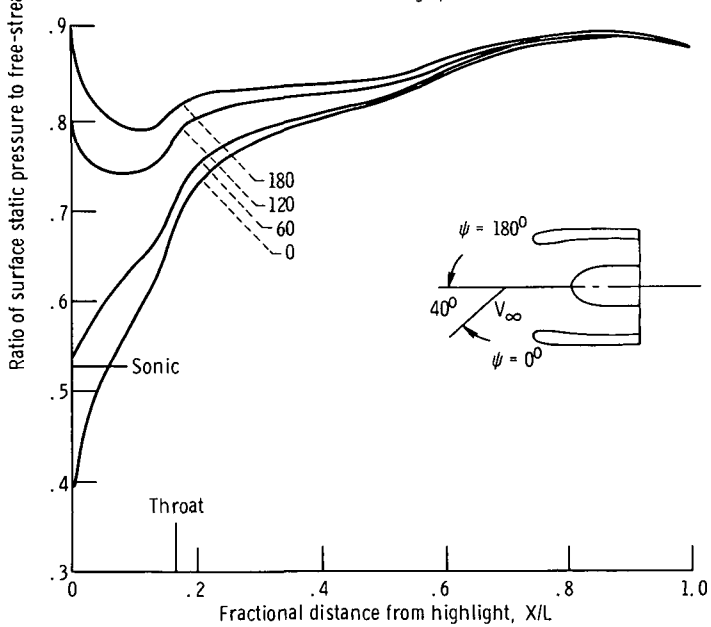

(b) Incidence angle, 40^0.

Figure 4. - Theoretical surface static-pressure distributions for various circumferential angles. Free-stream velocity, 32 meters per second; mass flow rate, 91 percent of design.

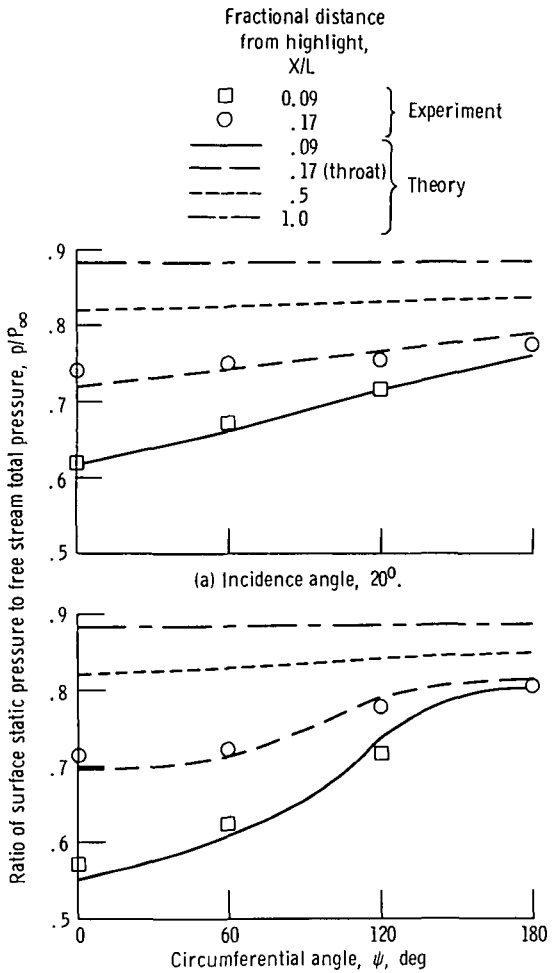

(a) Incidence angle, 20^0.

(b) Incidence angle, 40^0.

Figure 5. - Circumferential variation of surface static pressures for constant X/L locations. Free-stream velocity, 32 meters per second; mass flow rate, 91 percent of design.

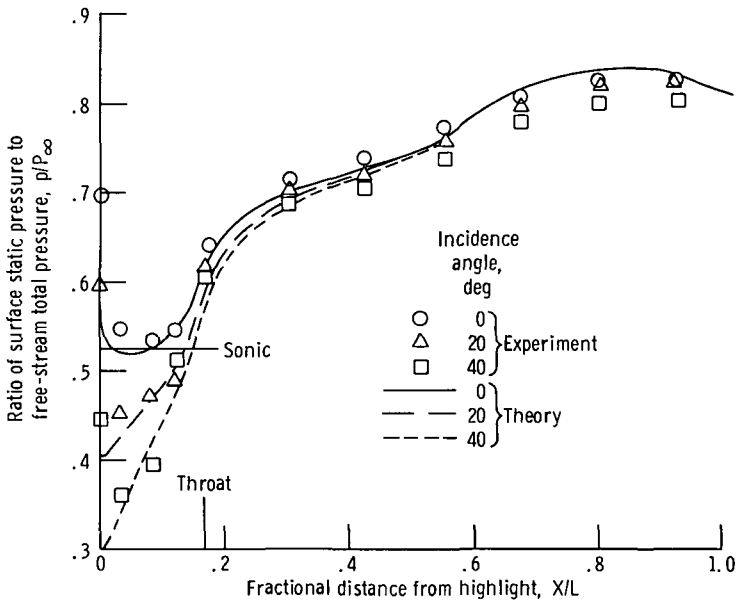

Figure 6. - Effect of incidence angle on surface static-pressure distributions. Free-stream velocity, 32 meters per second; mass flow rate, 103 percent of design; circumferential angle, 0; centerbody retracted.

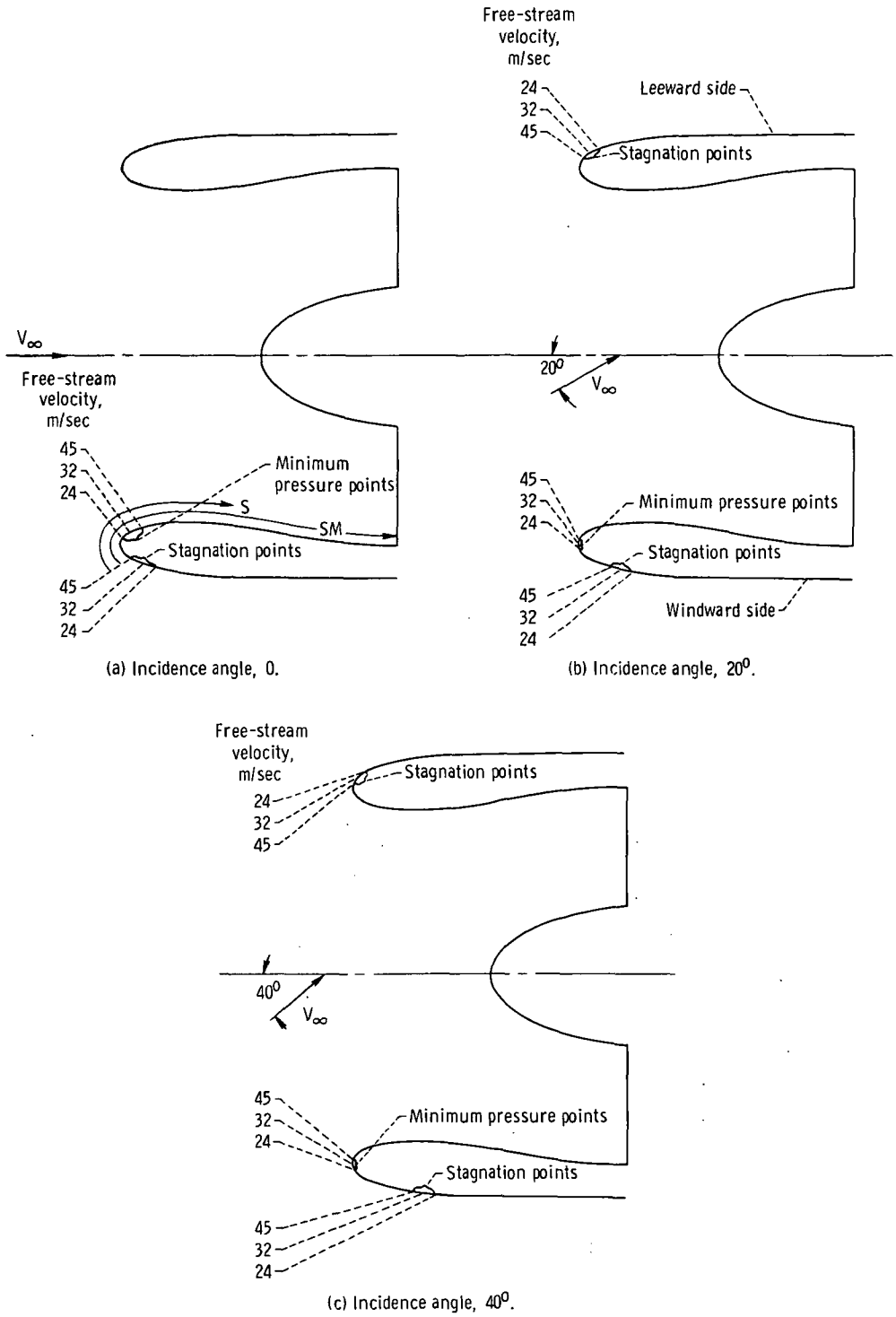

Figure 7. - Location of stagnation points and minimum pressure points. Mass flow rate, approximately, 100 percent of design.

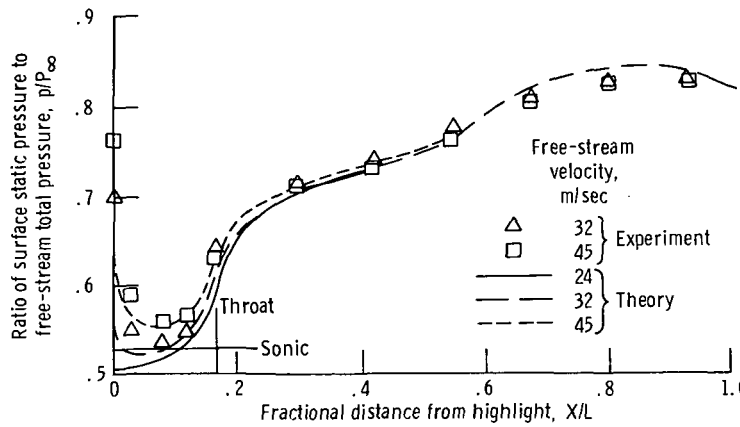

Figure 8. - Effect of free-stream velocity on surface static-pressure distributions. Incidence angle, 0; mass flow rate, 103 percent of design; circumferential angle, 0; centerbody retracted.

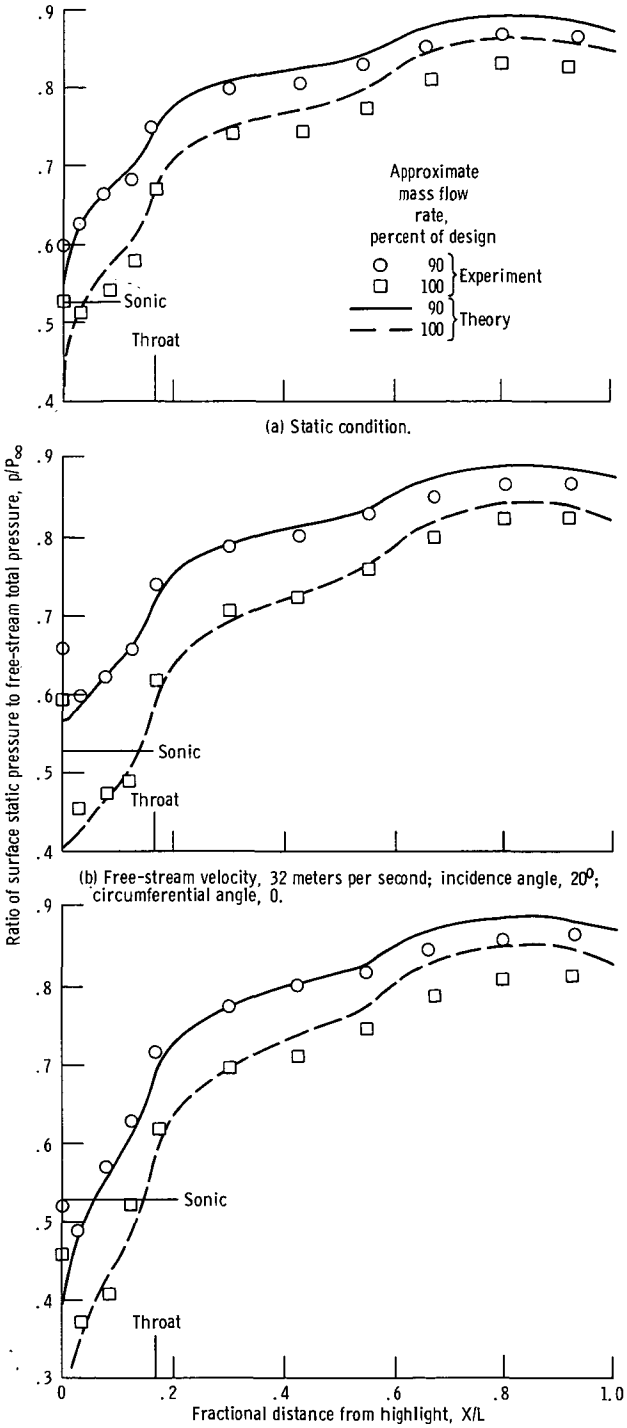

(a) Static condition.

(b) Free-stream velocity, 32 meters per second; incidence angle, 20°; circumferential angle, 0.

(c) Free-stream velocity, 32 meters per second; incidence angle, 40°; circumferential angle, 0.

Figure 9. - Effect of mass flow rate on surface static-pressure distributions. Centerbody retracted.

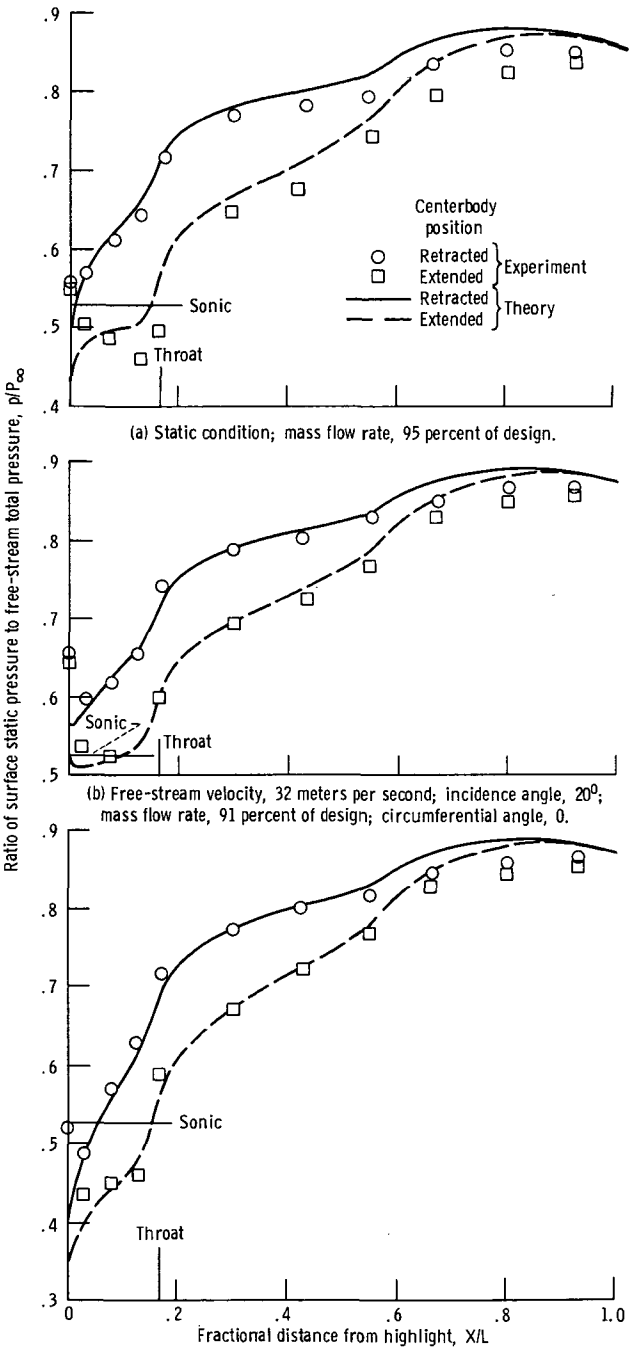

(a) Static condition; mass flow rate, 95 percent of design.

(b) Free-stream velocity, 32 meters per second; incidence angle, 20°; mass flow rate, 91 percent of design; circumferential angle, 0.

(c) Free-stream velocity, 32 meters per second; incidence angle, 40°; mass flow rate, 91 percent of design; circumferential angle, 0.

Figure 10. - Effect of centerbody position on surface static pressure distributions.

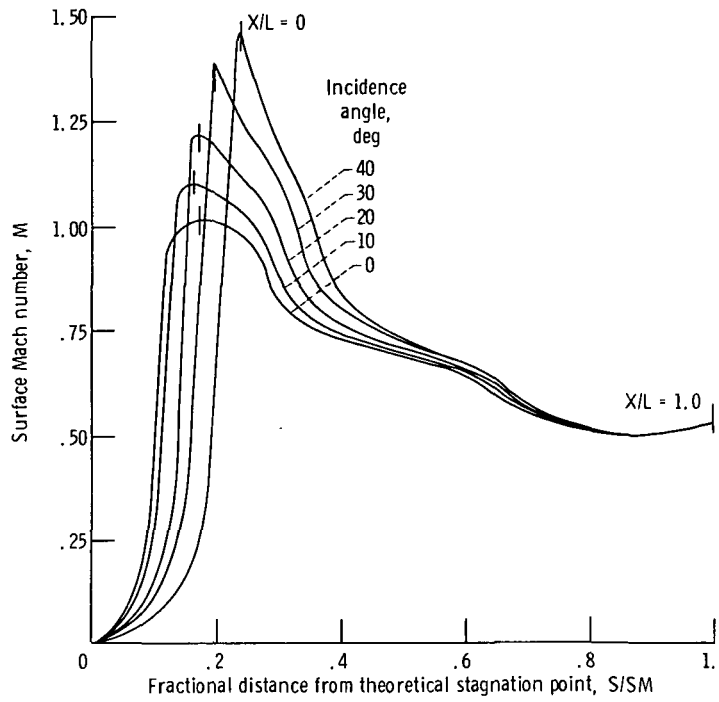

Figure 11. - Theoretical surface Mach number distributions. Free-stream velocity, 32 meters per second; mass flow rate, 103 percent of design; circumferential angle, 0.

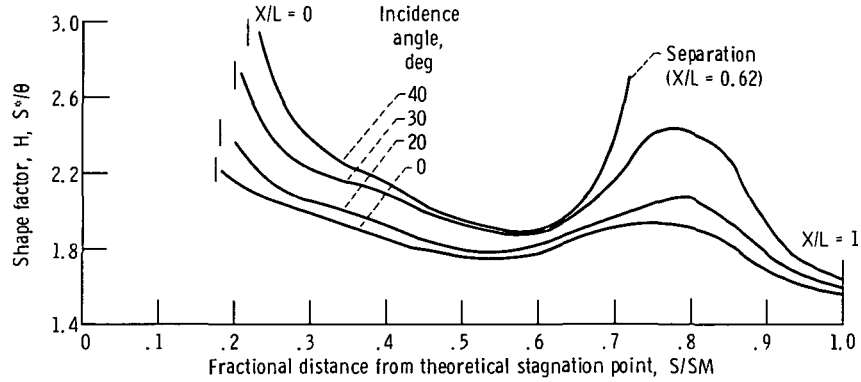

Figure 12. - Theoretical turbulent boundary-layer shape factor. Model scale; free-stream velocity, 32 meters per second; mass flow rate, 103 percent of design, circumferential angle, 0.

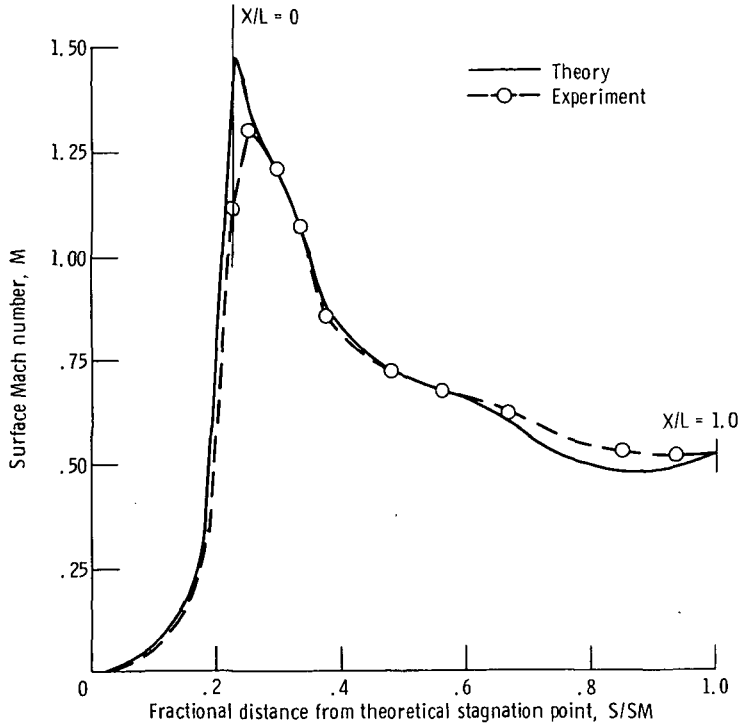

Figure 13. - Comparison of theoretical and experimental Mach number distributions. Free-stream velocity, 32 meters per second; incidence angle, 40^{0}; mass flow rate, 103 percent of design; circumferential angle, 0.

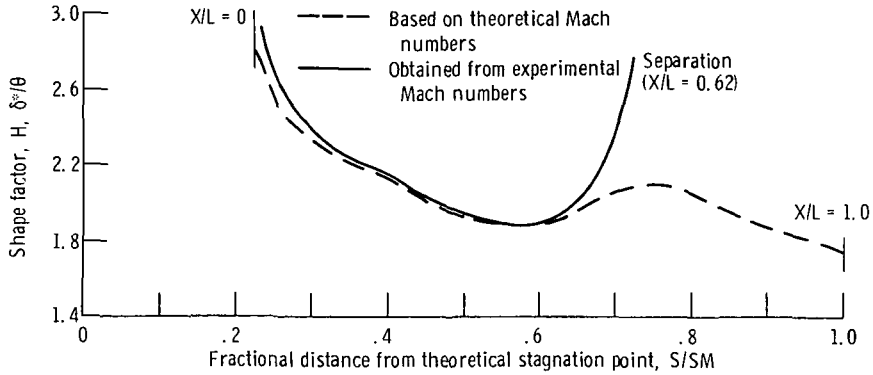

Figure 14. - Effect of theoretical and experimental Mach number distributions on theoretical turbulent boundary-layer shape factor. Model scale; free-stream velocity, 32 meters per second; incidence angle, 40^{0}; mass flow rate, 103 percent of design; circumferential angle, 0.

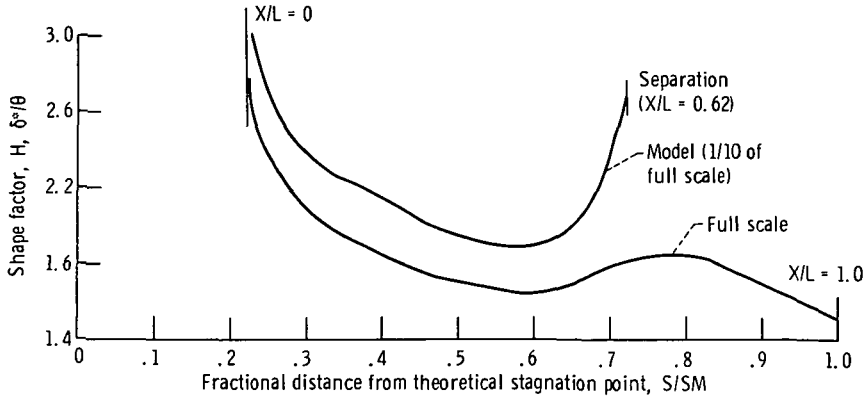

Figure 15. - Scale effect on theoretical turbulent boundary layer shape factor. Free-stream velocity, 32 meters per second; mass flow rate, 103 percent of design; incidence angle, 40°; circumferential angle, 0.

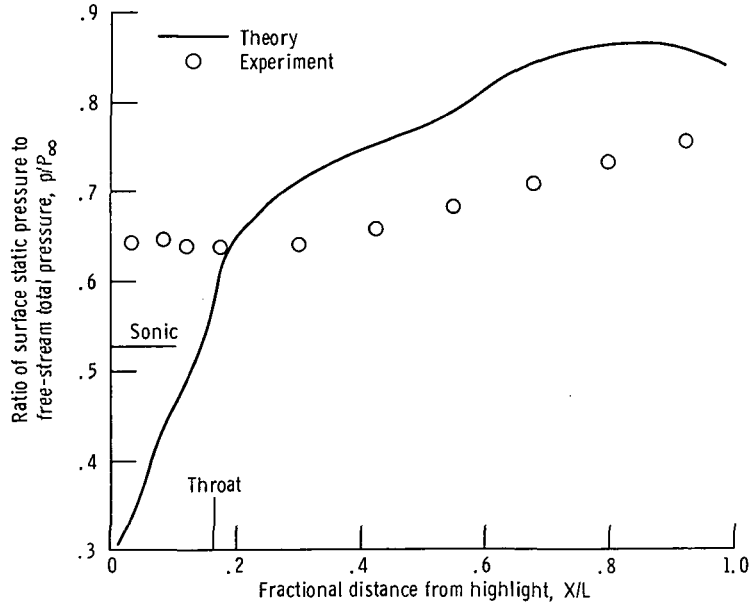

Figure 16. - Surface static-pressure distributions for separated flow. Incidence angle, 50°; free-stream velocity, 32 meters per second; mass flow rate, 100 percent of design; circumferential angle, 0.

"The aeronautical and space activities of the United States shall be conducted so as to contribute . . . to the expansion of human knowledge of phenomena in the atmosphere and space. The Administration shall provide for the widest practicable and appropriate dissemination of information concerning its activities and the results thereof."

—NATIONAL AERONAUTICS AND SPACE ACT OF 1958

NASA SCIENTIFIC AND TECHNICAL PUBLICATIONS

TECHNICAL REPORTS: Scientific and technical information considered important, complete, and a lasting contribution to existing knowledge.

TECHNICAL NOTES: Information less broad in scope but nevertheless of importance as a contribution to existing knowledge.

TECHNICAL MEMORANDUMS: Information receiving limited distribution because of preliminary data, security classification, or other reasons. Also includes conference proceedings with either limited or unlimited distribution.

CONTRACTOR REPORTS: Scientific and technical information generated under a NASA contract or grant and considered an important contribution to existing knowledge.

TECHNICAL TRANSLATIONS: Information published in a foreign language considered to merit NASA distribution in English.

SPECIAL PUBLICATIONS: Information derived from or of value to NASA activities. Publications include final reports of major projects, monographs, data compilations, handbooks, sourcebooks, and special bibliographies.

TECHNOLOGY UTILIZATION PUBLICATIONS: Information on technology used by NASA that may be of particular interest in commercial and other non-aerospace applications. Publications include Tech Briefs, Technology Utilization Reports and Technology Surveys.

Details on the availability of these publications may be obtained from:

SCIENTIFIC AND TECHNICAL INFORMATION OFFICE

NATIONAL AERONAUTICS AND SPACE ADMINISTRATION

Washington, D.C. 20546